

# ornl

ORNL-/TM-11060

**OAK RIDGE  
NATIONAL  
LABORATORY**

**MARTIN MARIETTA**

## The Physics of Compensating Calorimetry and the New CALOR89 Code System

T. A. Gabriel  
J. E. Brau  
B. L. Bishop

OAK RIDGE NATIONAL LABORATORY

CENTRAL RESEARCH LIBRARY

CIRCULATION SECTION

400N. ROOM 171

**LIBRARY LOAN COPY**

DO NOT TRANSFER TO ANOTHER PERSON

If you wish someone else to see this  
report, send to name with report and  
the library will arrange a loan.

OPERATED BY  
MARTIN MARIETTA ENERGY SYSTEMS, INC.  
FOR THE UNITED STATES  
DEPARTMENT OF ENERGY

Printed in the United States of America. Available from  
National Technical Information Service  
U.S. Department of Commerce  
5285 Port Royal Road, Springfield, Virginia 22161  
NTIS price codes—Printed Copy: A03; Microfiche A01

This report was prepared as an account of work sponsored by an agency of the United States Government. Neither the United States Government nor any agency thereof, nor any of their employees, makes any warranty, express or implied, or assumes any legal liability or responsibility for the accuracy, completeness, or usefulness of any information, apparatus, product, or process disclosed, or represents that its use would not infringe privately owned rights. Reference herein to any specific commercial product, process, or service by trade name, trademark, manufacturer, or otherwise, does not necessarily constitute or imply its endorsement, recommendation, or favoring by the United States Government or any agency thereof. The views and opinions of authors expressed herein do not necessarily state or reflect those of the United States Government or any agency thereof.

ORNL/TM-11060

Engineering Physics and Mathematics

**The Physics of Compensating Calorimetry  
and the New CALOR89 Code System**

T. A. Gabriel, J. E. Brau,\* and B. L. Bishop

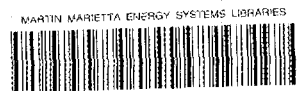
\*Dept. of Physics, University of Oregon

Prepared for Office of High Energy & Nuclear Physics

DATE PUBLISHED — March 1989

**NOTICE:** This document contains information of a preliminary nature. It is subject to revision or correction and therefore does not represent a final report.

Prepared by the  
OAK RIDGE NATIONAL LABORATORY  
Oak Ridge, Tennessee 37831  
operated by  
MARTIN MARIETTA ENERGY SYSTEMS, INC.  
for the  
U.S. DEPARTMENT OF ENERGY  
under contract DE-AC05-84OR21400



3 4456 0284646 4



## CONTENTS

ABSTRACT . . . . .	v
1. INTRODUCTION . . . . .	1
2. FUNDAMENTAL PHYSICS OF COMPENSATING CALORIMETERS . . . . .	3
3. METHOD OF CALCULATIONS . . . . .	5
4. RESULTS . . . . .	9
5. CONCLUSIONS . . . . .	18
REFERENCES . . . . .	19



## ABSTRACT

Much of the understanding of the physics of calorimetry has come from the use of excellent radiation transport codes. A new understanding of compensating calorimetry was introduced four years ago following detailed studies with a new CALOR system. Now, the CALOR system has again been revised to reflect a better comprehension of high energy nuclear collisions (HETC88) by incorporating a modified high energy fragmentation model from FLUKA87. This revision will allow for the accurate analysis of calorimeters at energies of 100's of GeV. Presented in this paper is a discussion of compensating calorimetry, the new CALOR system (CALOR89), the revisions to HETC, and recently generated calorimeter related data on modes of energy deposition and secondary neutron production ( $E < 50$  MeV) in infinite iron and uranium blocks.



# 1. INTRODUCTION

Four years ago, a paper was presented detailing the underlying mechanisms of compensating calorimetry.<sup>1</sup> From previous presentations and publications,<sup>2,3</sup> it was recognized at that time that this new understanding would be met with much skepticism within the high-energy physics community. At that time, the following critical points were deduced following substantial analysis of various calorimeter systems utilizing the then current CALOR system:<sup>4</sup>

1. prior to later experimental confirmation, it was pointed out that current designs of uranium liquid argon calorimeters were not fully compensating;<sup>1,2,3,5,6</sup>
2. the importance of the hydrogen content in the active medium to couple the low energy neutrons to the output signal was stressed;<sup>1,2,3,5,6</sup>
3. the significant role of "electromagnetic sampling inefficiencies" (which are the result of preferential photon absorption<sup>7</sup> and electron multiple scattering in the high-Z inactive material<sup>3,6</sup>) in reducing the ratio of electron to hadron response was explained;<sup>1,2,3,5,6</sup>
4. the importance of the saturation of signal in the regions of high density energy deposition was emphasized;<sup>1,2,3,5,6</sup> and
5. these new understandings led us to "predict that a lead calorimeter may also give EM/HAD  $\approx 1$ ",<sup>8</sup> where EM/HAD is the ratio of average electron-to-hadron response for the same incident kinetic energy, hereafter referred to as the e/h ratio. In other words, a compensating lead calorimeter was predicted.

As a result of these predictions, experimental programs (for example,<sup>9</sup> SLD and DO uranium liquid argon and uranium-scintillator tests) directed their efforts at proving or disproving the above conclusions. After much experimental testing and reviewing, as well as additional analytical efforts<sup>10,11</sup> during the past four years, this skepticism has evolved into a general acceptance by the community of this new understanding of compensating calorimetry.<sup>12</sup>

This new enlightenment was a direct result of having in hand a code system, CALOR,<sup>4</sup> which contained as good a description of the current physics of calorimetry as possible. However, there is still substantial room for improvements in all calorimeter code systems. Current and future improvements in these code systems will provide additional returns through better designs of calorimeters, as well as a better understanding of the physics processes at SSC energies. The HETC module of the CALOR system has now been modified through the inclusion of a better high energy collision model<sup>13</sup> (that of FLUKA87) while retaining the excellent low energy treatment of the old CALOR system. With this new hybrid model, the response of various calorimeters can now be studied at energies of hundreds of GeV with confidence that both the high energy and the low energy descriptions are sound.

Presented in the following sections is a brief summary of the understanding of compensating calorimetry, a description of the new CALOR code system, and recently obtained data using the new CALOR system. In particular, data have been obtained to determine the mode of energy deposition and secondary particle production, specifically neutrons produced with energies less than 50 MeV, in

infinite iron and uranium blocks. Also, comparisons are made with the older version of CALOR.

## 2. FUNDAMENTAL PHYSICS OF COMPENSATING CALORIMETERS

The first requirements of a sampling hadron calorimeter are that it is large enough to contain most of the hadronic shower and that it have frequent enough samples that sampling fluctuations are small. Once these requirements are met, the two most important parameters of a hadron calorimeter, the energy resolution and the ratio of the most probable signal from an electron to that from a hadron of the same energy ( $e/h$ ), will be dominated by fluctuations in the hadron shower and losses due to nuclear binding energy. In sampling calorimeter design, it was once assumed that the active medium samples the shower in the passive medium in detail and that for both the incident radiation, and the secondary radiation, the signal output from the active medium is the same fixed fraction of the energy deposited in the passive medium. While this is approximately true for electromagnetic calorimeters, it is far from the truth for hadron calorimeters. In practice, however, the active and passive media exhibit different characteristics when exposed to similar types of radiation. The active media often do not give similar response for the same energy deposition by different particles and the energy sampling is not equal in the active region for electrons, gamma rays, low-energy neutrons, and charged hadrons. Calorimeters which utilize iron or low atomic weight ( $A$ ) materials as the passive media exhibit an almost equal distribution of the cascade energy into protons, neutrons, charged pions and neutral pions for intermediate incident energy (1-20 GeV) hadrons. On the contract, if Pb, Ta, or U is used as the passive material, the energy distribution among produced particles is shifted toward additional neutron production through spallation and fission. There are also more secondary particles and the energy spectra of all of them are shifted toward lower energies. In calorimeters utilizing low  $A$  materials, the majority of the energy flow is from charged particles which are produced in the passive material and which pass through the active region. In calorimeters utilizing high  $A$  material, the energy flow from charged particles produced in the passive material is reduced relative to that due to the neutral particles, in particular, low energy cascade neutrons of energy 1-20 MeV. To fully utilize the sizable fraction of energy left in the cascade due to these neutrons of energy less than 20 MeV, the detection medium itself must be sensitive through internal collisions with these particles. It is also possible to deliberately enhance the signal due to these low energy neutrons, relative to the signal from other particles by using an active medium which detects these neutrons with greater efficiency than the passive medium. On the other hand, low energy recoil protons or other heavier ions of a given energy produce in many detectors, a smaller signal than electrons or gamma rays of the same energy, thereby reducing their effectiveness.<sup>14</sup>

One way of enhancing the sensitivity to low energy neutrons is by using a hydrogenous active medium.<sup>1,3,5</sup> Hydrogen has a large cross section for neutron scattering, on the order of several  $\times 10^{-24}$  cm<sup>2</sup> for neutrons of energy of a few MeV. Hydrogen also allows for the largest energy transfer in elastic scattering.<sup>1,3,5</sup> Proton production via nonelastic neutron collision with other nuclei in the active media will only consume binding energy and will not help substantially with the signal. With equal sensitivity of the active media to gamma rays, electrons, and neutrons, it can be shown that the choice of a hydrogenous active medium and

a passive medium with high atomic number can overcompensate for the loss of hadron pulse height due to nuclear binding energy and lead to an  $e/h$  ratio less than unity.<sup>1</sup> The knowledge of this led Brückmann<sup>10</sup> to introduce “tuning” by varying the relative thickness of active and passive material.

The use of uranium, as first suggested by Fabjan and Willis<sup>15</sup> offers a way to compensate, i.e., to make  $e/h = 1$  and improve the resolution on an event-by-event basis for hadronic shower fluctuations and losses due to nuclear binding energy. These improvements can be understood from an examination of the hadronic cascade. In noncompensating calorimeters, particle cascades which are strongly electromagnetic due to extensive neutral pion content will give significantly larger signals than cascades lacking in electromagnetic source. This results since the latter type of cascade tends to involve large numbers of hadronic particles which lead to many collisions which lose binding energy. These cascades also contain poorly detected low energy nucleons. Consequently, the fluctuations in particle type translate to fluctuation in observed energy. Consider, however, a uranium calorimeter. If the particle cascade is strongly electromagnetic in character, the uranium will tend to suppress the electromagnetic part of the cascade due to sampling inefficiencies,<sup>6,12</sup> that is, a larger fraction of the energy will be deposited in the U than would be expected by a simple analysis (see point 3 in the Introduction). However, if the cascade is strongly hadronic, there will be an amplification of the low energy neutrons and, to a lesser extent, gamma ray energy from hadronically produced cascade neutrons and fission neutrons, and neutron induced fission, capture, and inelastic collisions. Sampling inefficiencies are not as large for pure hadronic cascades, therefore the signal remains less affected. The combination of electromagnetic suppression and little hadronic suppression improves the resolution by narrowing the pulse height. However, if the active medium is not very sensitive to low energy neutrons only sampling inefficiencies will contribute to improvements in compensation; i.e., improvements in the  $e/h$  ratio. If liquid argon is chosen as the active medium, signals from the low energy neutron collisions with the argon atoms will be greatly suppressed due to saturation effects and small energy transfer.<sup>1,3,5</sup> If plastic, TMS, or TMP is chosen, the hydrogen will enhance the low energy neutron signal due to the produced proton recoils, as mentioned earlier. However, saturation effects due to the inefficient light or charge production mechanism for low energy protons can limit their effectiveness. This increased neutron signal will also tighten the pulse height distribution thereby improving the energy resolution and in addition will reduce the  $e/h$  ratio. It should be noted that overcompensation can occur and then the resolution will become worse. The resolution should be at a minimum when  $e/h \approx 1$ . Further details on this discussion can be found in Ref. 12.

### 3. METHOD OF CALCULATIONS

The calculations presented in this paper were performed with the new CALOR computer system following approximately the procedures used in previous calculations.<sup>1,5</sup> The major changes in CALOR are in an improved high energy collision model following FLUKA87 and a better low energy neutron transport by the code MICAP. A flow diagram of the codes in CALOR is given in Fig. 1. The three-dimensional, multimedia, high-energy nucleon-meson transport code HETC88<sup>16,17,18</sup> was used, with modifications, to obtain a detailed description of the nucleon-meson cascade produced in the absorbers considered in this paper. This Monte Carlo code takes into account the slowing down of charged particles via the continuous slowing-down approximation, the decay of charged pions and muons, inelastic nucleon-nucleus and charged-pion-nucleus (excluding hydrogen) collisions through the use of an intermediate-energy intranuclear-cascade evaporation (MECC) model ( $E < 3$  GeV), a scaling model ( $3 \text{ GeV} < E < 5$  GeV), and a multi-chain fragmentation model ( $E > 5$  GeV), and inelastic nucleon-hydrogen and charged-pion-hydrogen collisions via the isobar model ( $E < 3$  GeV), and a fragmentation model ( $E > 3$  GeV). Also accounted for are elastic neutron-nucleus ( $E < 100$  MeV) collisions, and elastic nucleon and charged-pion collisions with hydrogen.

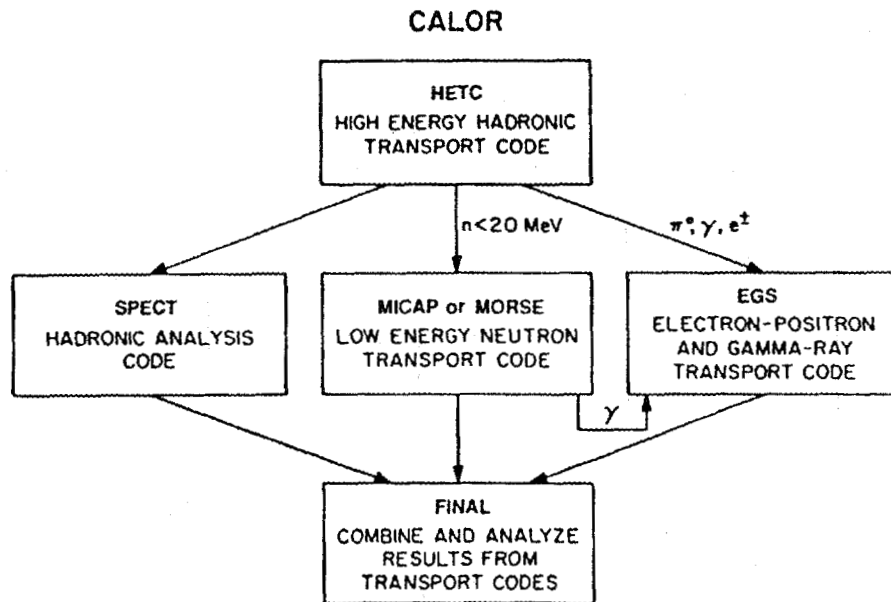


Fig. 1. Flow diagram of the CALOR computer system.

The intranuclear-cascade-evaporation model as implemented by Bertini is the low energy (20-3000 MeV) heart of the HETC code.<sup>19</sup> This model has been used for a variety of calculations and has been shown to agree quite well with many experimental results. The underlying assumption of this model is that particle-nucleus interactions can be treated as a series of two-body collisions within the nucleus and that the location of the collision and resulting particles from the collision are governed by experimental and/or theoretical particle-particle total and differential cross-section data. The types of particle collisions included in the calculations are elastic, nonelastic and charge exchange. This model incorporates the diffuseness of the nuclear edge, the Fermi motion of the bound nucleons, the exclusion-principle, and a local potential for nucleons and pions. The density of the neutrons and protons within the nucleus (which is used with the total cross sections to determine interaction locations) are determined from the experimental data of Hofstadter.<sup>19</sup> Nuclear potentials are determined from these density profiles by using a zero-temperature Fermi distribution. The total well depth is then defined as the Fermi energy plus 7 MeV. Following the cascade part of the interaction, excitation energy remains in the nucleus. This energy is treated by using an evaporation model which allows for the emission of protons, neutrons, d,  $^3\text{He}$ ,  $\alpha$  and t. Fission, induced by high-energy particles, is accounted for during this phase of the calculation by allowing it to compete with evaporation. Whether or not a detailed fission model is included has very little effect on the total number of secondary neutrons produced.

In recent years, a large amount of experimental and theoretical work has been done, and more reliable models are now available for the description of high energy ( $\geq 5$ -10 GeV) hadron-proton and hadron-nucleus collisions. In particular, a multi-chain fragmentation model of hadron-nucleus collisions has been developed and implemented into a Monte Carlo code by J. Ranft et al.,<sup>20</sup> following the work of A. Capella and J. Tran Thanh Van.<sup>21</sup> The version of the model that is used in the work reported here, with some modifications, is that provided by the transport code FLUKA87. The modifications that have been made are mostly those necessary to predict such things as residual nuclei and excitation energies.<sup>22</sup> This information is needed in HETC for evaporation calculations which yield the production of low-energy neutrons, protons, deuterons, alpha particles, etc.

At high energies, a complete intranuclear cascade does not develop when a nucleon is hit by a hadronic projectile inside the nucleus. The time-scale governing typical hadronic interactions is very long and therefore the most energetic secondaries are actually produced as the jet decays beyond the target nucleus and therefore have no chance of re-scattering.

EVENTQ is the hadron-nucleus collision code taken from FLUKA. In this code, a simplified Monte Carlo model is used in which no tracking or cascading of particles occurs.

As a first step, some energy is subtracted from the original projectile energy to account for intranuclear cascade nucleons which are chosen from distributions. The remaining energy is given to the projectile, which keeps its original direction. The momenta of the cascade particles are taken to be isotropic so that at this step momentum is conserved only on the average.

For initial momenta greater than 5 GeV/c, the average number of collisions inside the nucleus is taken from multiple scattering theory.<sup>23,24,25</sup> The actual number

of collisions is chosen randomly from an exponential-appearing distribution due to Nilsson and Stenlund,<sup>26</sup> based on a simplified Monte Carlo collision calculation.

The theory of Capella<sup>27</sup> is followed in defining these collisions. In Ranft's version only one collision occurs using the valence quarks of the projectile. The remaining collisions occur with the "projectiles" being pi-zero-like mesons composed of parton sea quarks of the original projectile.

The total energy of each meson is given by

$$E_{sea} = E_{kin_{proj}}(X_q + X_{aq}) \quad (1)$$

where  $E_{kin_{proj}}$  is the original kinetic energy of the original projectile diminished by the total energies of mesons already chosen;  $X_q$  and  $X_{aq}$  are the energy fractions of the quark and antiquark in the meson. Each  $X$  is chosen from the distribution

$$d(X) \approx (1 - X)^a / X^b \quad (2)$$

with  $a = 4$  and  $b = 1$ .

The target nucleons are assumed to exist in a one-region nuclear well, from which the Fermi momentum is chosen.<sup>28</sup>

In EVENTQ87,\* diffractive hadron-hadron collisions<sup>29,30</sup> are included at this stage, occurring randomly 30% of the time. Basically, the target or "projectile" hadron (possibly a meson composed of sea quarks) interacts only via its sea quarks, the valence quarks reconstituting to the original hadron, which does not collide.

In the C.M.S. of the current projectile and target, two jets (chains) are formed. In EVENTQ82, these jets may be quark-antiquark, quark-diquark, or diquark-antidiquark jets, and are formed only from valence quarks of the target. The theory is based on jet formation in electron-positron and lepton-hadron collisions. In EVENTQ87, additional jets may also be formed using sea quarks of the target.<sup>31</sup>

If ECM is the center of mass energy, the fractions of ECM/2 for single valence quarks of projectile and target,  $X_p$  and  $X_t$ , are chosen from Eq. (2) with  $b = 1/2$  and  $a = 5/2$  for baryons,  $a = 1/2$  for mesons, in EVENTQ82. In EVENTQ87,  $a = 1$  for baryons,  $a = 1/2$  for mesons. The remaining fractions for the antiquark or diquark are given by  $XX_p = 1 - X_p$ ;  $XX_t = 1 - X_t$ . The two jet energies are then

$$E_1 = \frac{ECM}{2}(X_t + XX_p); E_2 = \frac{ECM}{2}(X_p + XX_t) \quad (3)$$

with the sum  $E_1 + E_2 = ECM$ . The momenta are given by

$$P_1 = \frac{ECM}{2}(XX_p - X_t); P_2 = \frac{ECM}{2}(X_p - XX_t) \quad (4)$$

and  $P_1 = -P_2$ . The jet masses are obtained as  $m^2 = E^2 - P^2$ .

If the masses are too small for fragmentation, stable particle masses are assigned. Two masses are enough to determine the energies and total momenta in the C.M.S.

---

\* EVENTQ87 is the latest version of EVENTQ and is the one incorporated into HETC88. EVENTQ82 is an earlier version used in FLUKA82.

Transverse momenta are also assigned in some cases in EVENTQ82 and all cases in EVENTQ87.

Fragmentation of the jets in the jet C.M.S. is carried out, with possible formation of 180 stable particles or resonances.<sup>32</sup> The resonances decay with either two-body isotropic decay or three-body decay. Experimental decay products and branching ratios are input<sup>33</sup> to the code so that all quantum numbers are conserved. In this way, exclusive events are generated, and correlation studies can be carried out. All particles produced in the fragmentation of the jets are assumed not to interact with the nucleus.<sup>13,23</sup>

The source distribution for the electromagnetic cascade calculation is provided by HETC; it consists of direct photon production from hadron-nuclear collisions, photons from neutral pion decay, electrons and positrons from muon decay (although this is usually not of interest in calorimeter calculations because of the long muon lifetime), de-excitation gamma rays from nonelastic nuclear collisions and fission gamma rays. Since the discrete decay energies of the deexcitation gammas are not provided by HETC and only the total energy is known, individual gamma energies are obtained by uniformly sampling from the available energy until it is completely depleted. The transport of the electrons, positrons, and gammas from the above sources is carried out using the EGS system.<sup>34</sup>

Neutrons which are produced with energies below 20 MeV are transported using the MORSE<sup>35,36</sup> or MICAP<sup>37</sup> Monte Carlo transport codes. The neutron cross sections used by MORSE or MICAP are obtained from ENDFB/V. Gamma rays (including those from capture, fission, etc.) produced during this phase of the calculations are stored for transport by the EGS code. The MORSE code was developed for reactor application. The MICAP code was developed specifically for detector analysis. Both codes can treat fissioning systems in detail. This ability is very important since a majority of the fissions results from neutrons with energies less than 20 MeV. Time dependence is included in MORSE and MICAP, but since neither HETC nor EGS has a timing scheme incorporated, it is generally assumed that no time passes for this phase of the particle cascade. Therefore, all neutrons below 20 MeV are produced at  $t = 0$ . General time cuts used in the MORSE or MICAP codes are 50 ns for scintillator and 100 ns for TMS or Argon.

The nonlinearity of the light pulse,  $L$ , in scintillator due to saturation effects is taken into account by the use of Birk's law<sup>14</sup>

$$\frac{dL}{dx} \propto \frac{dE/dx}{1 + k_B dE/dx},$$

where  $k_B$  is the saturation constant. For plastic scintillator  $k_B$  is generally between 0.01- and 0.02-g cm<sup>2</sup> MeV<sup>-1</sup>. A similar law is assumed to apply to the charge collected in ionization detectors. This takes into account the loss of signal resulting from recombination effects in the ionization column.<sup>38</sup> For electrons at all energies, it is assumed that  $k_B = 0$ .

## 4. RESULTS

Calorimeter response is very sensitive to the amount of energy appearing as electromagnetic or hadronic, as well as the amount of energy which is effectively lost; for example, binding energy, nuclear recoil, evaporated charged particles (only in the inactive material for sampling calorimeters), and neutrino energy. Presented in Tables 1-5 are data which represent the breakdown of energy deposition and production in infinite iron and uranium targets. The data are also given graphically in Figs. 2-4. The data presented include the energy deposition due to the primary protons and the produced secondary protons, pions, and muons. These four energy depositions given in the tables are summed to yield the B curves in Figs. 2-4. Also presented in the tables is the energy produced in the electromagnetic channel either from  $\pi^0$  or gamma production during the initial phase of a nuclear collision or deexcitation gamma rays that appear at a slower rate, usually following the evaporation phase of the collision. These two energy productions are summed to yield the A curves in Figs. 2-4. The energy produced in the form of low energy (<50 MeV) neutrons is also given in the table and is represented as curve D in the figures. These neutrons have not been transported, but represent the source distribution which would be used in transport codes such as MORSE or MICAP. The remainder of the data represent lost energy with respect to calorimeter application, i.e., binding and neutrino energy, electron energy from muon decay and heavy ion ( $A > 1$ ) recoil energy. These values are summed to yield curve C in the figures.

Table 1  
 Calculated Energy Deposition, Binding Energy Losses, and  
 Neutron Production ( $E < 50$  MeV) in an Infinite Iron Target  
 for 1.-, 2.-, 4.95-, and 5.05-GeV Source Protons Using the HETC88 Code.

<u>Energy Type</u>	<u>Proton Energy (GeV)</u>			
	1	2	4.95	5.05
Primary ionization	0.195	0.170	0.185	0.194(0.209) <sup>d</sup>
Secondary protons	0.385	0.744	1.67	1.69(1.70)
Secondary charged pions <sup>a</sup>	0.0188	0.117	0.409	0.376(0.397)
Secondary muons	0.0001	0.0006	0.003	0.003(0.006)
Excitation gammas <sup>b</sup>	0.0230	0.0410	0.108	0.101(0.103)
Neutral pions and high energy gammas	0.0411	0.191	0.805	0.919(0.853)
Heavy ion recoil	0.0177	0.0465	0.125	0.108(0.128)
Binding and neutrino energy and electron energy from muon decay	0.215	0.463	1.08	1.12(1.08)
Energy of neutrons produced with energy less than 50 MeV <sup>c</sup>	0.104	0.226	0.561	0.538(0.570)
Neutrons produced per GeV ( $E < 50$ MeV)	13.0	13.2	12.8	12.2(12.6)

<sup>a</sup> In this version of HETC, all kaons, anti-protons, etc., are converted to charged pions before transport.

<sup>b</sup> Energy remaining in nucleus after collisions involving all charged particles and neutrons with energies  $> 50$  MeV.

<sup>c</sup> This is the total energy contained in neutrons with energies less than 50 MeV. If these particles were transported until capture, the binding energy would reduce by  $\sim$  the number of neutrons times 7 MeV.

<sup>d</sup> Values in parentheses are those obtained using the old version of HETC. For energies less than 5 GeV, the old version of HETC is equivalent to the new version.

Table 2  
 Calculated Energy Deposition, Binding Energy Losses, and  
 Neutron Production ( $E < 50$  MeV) in an Infinite Iron Target  
 for 10-, 20-, and 50-GeV Source Protons Using the HETC88 Code.

<u>Energy Type</u>	<u>Proton Energy (GeV)</u>		
	10	20	50
Primary ionization	0.218(0.205) <sup>d</sup>	0.219(0.214)	0.253(0.258)
Secondary protons	2.63(3.36)	4.70(6.40)	9.53(14.8)
Secondary charged pions <sup>a</sup>	0.996(0.873)	2.09(1.65)	5.07(4.03)
Secondary muons	0.007(0.019)	0.016(0.037)	0.039(0.061)
Excitation gammas <sup>b</sup>	0.166(0.210)	0.309(0.397)	0.641(0.930)
Neutral pions and high energy gammas	3.02(1.89)	7.19(4.99)	23.1(14.8)
Heavy ion recoil	0.150(0.248)	0.274(0.457)	0.557(1.26)
Binding and neutrino energy and electron energy from muon decay	1.96(2.12)	3.66(3.89)	7.61(9.15)
Energy of neutrons produced with energy less than 50 MeV <sup>c</sup>	0.848(1.07)	1.54(1.96)	3.19(4.66)
Neutrons produced per GeV ( $E < 50$ MeV)	9.78(12.4)	8.92(11.6)	7.45(10.8)

<sup>a</sup> In this version of HETC, all kaons, anti-protons, etc., are converted to charged pions before transport.

<sup>b</sup> Energy remaining in nucleus after collisions involving all charged particles and neutrons with energies  $> 50$  MeV.

<sup>c</sup> This is the total energy contained in neutrons with energies less than 50 MeV. If these particles were transported until capture, the binding energy would reduce by  $\sim$  the number of neutrons times 7 MeV.

<sup>d</sup> Values in parentheses are those obtained using the old version of HETC. For energies less than 5 GeV, the old version of HETC is equivalent to the new version.

Table 3  
 Calculated Energy Deposition, Binding Energy Losses, and  
 Neutron Production ( $E < 50$  MeV) in an Infinite Iron Target  
 for 100-, 200-, and 500-GeV Source Protons Using the HETC88 Code.

<u>Energy Type</u>	<u>Proton Energy (GeV)</u>		
	100.	200.	500.
Primary ionization	0.240(0.266) <sup>d</sup>	0.267(0.165)	0.227
Secondary protons	16.7(28.8)	28.8(55.1)	57.6
Secondary charged pions <sup>a</sup>	9.97(8.05)	18.0(15.9)	37.6
Secondary muons	0.077(0.224)	0.141(0.232)	0.289
Excitation gammas <sup>b</sup>	1.16(1.80)	2.02(3.40)	4.09
Neutral pions and high energy gammas	51.6(31.8)	115.(68.6)	32.8
Heavy ion recoil	0.974(2.23)	1.81(5.87)	3.69
Binding and neutrino energy and electron energy from muon decay	13.6(17.8)	23.7(33.7)	48.1
Energy of neutrons produced with energy less than 50 MeV <sup>c</sup>	5.71(9.00)	10.0(17.1)	20.4
Neutrons produced per GeV ( $E < 50$ MeV)	6.68(10.5)	5.84(9.86)	4.74

<sup>a</sup> In this version of HETC, all kaons, anti-protons, etc., are converted to charged pions before transport.

<sup>b</sup> Energy remaining in nucleus after collisions involving all charged particles and neutrons with energies  $> 50$  MeV.

<sup>c</sup> This is the total energy contained in neutrons with energies less than 50 MeV. If these particles were transported until capture, the binding energy would reduce by  $\sim$  the number of neutrons times 7 MeV.

<sup>d</sup> Values in parentheses are those obtained using the old version of HETC. For energies less than 5 GeV, the old version of HETC is equivalent to the new version.

Table 4  
 Calculated Energy Deposition, Binding Energy Losses, and  
 Neutron Production ( $E < 50$  MeV) in an Infinite Uranium Target  
 for 1-, 2-, 4.95-, 5.05- and 10-GeV Source Protons Using the HETC88 Code.

<u>Energy Type</u>	<u>Proton Energy (GeV)</u>				
	1.0	2.0	4.95	5.05	10.0
Primary ionization	0.253	0.254	0.249	0.244	0.262
Secondary protons	0.220	0.489	1.15	1.14	2.02
Secondary charged pions <sup>a</sup>	0.012	0.077	0.277	0.308	0.944
Secondary muons	0.002	0.002	0.001	0.001	0.004
Excitation gammas <sup>b</sup>	0.013	0.026	0.063	0.063	0.101
Neutral pions and high energy gammas	0.042	0.121	0.578	0.624	2.43
Heavy ion recoil	0.018	0.632	0.187	0.183	0.192
Binding and neutrino energy and electron energy from muon decay	0.272	0.602	1.49	1.54	2.72
Energy of neutrons produced with energy less than 50 MeV <sup>c</sup>	0.168	0.368	0.951	0.950	1.33
Neutrons produced per GeV ( $E < 50$ MeV)	36.0	37.1	36.1	36.0	27.5
Number of fast fissions <sup>d</sup>	2.65	5.01	12.4	12.6	20.2

<sup>a</sup> In this version of HETC, all kaons, anti-protons, etc., are converted to charged pions before transport.

<sup>b</sup> Energy remaining in nucleus after collisions involving all charged particles and neutrons with energies  $> 50$  MeV.

<sup>c</sup> This is the total energy contained in neutrons with energies less than 50 MeV. If these particles were transported until capture, the binding energy would reduce by  $\sim$  the number of neutrons times 7 MeV.

<sup>d</sup> Fissions produced by all charged particles and neutrons with energy  $> 50$  MeV. To calculate the amount of prompt fission gamma energy multiply by 7.538 MeV/fission. The energy associated with fission is not included for calculating binding energy.

Table 5  
 Calculated Energy Deposition, Binding Energy Losses, and  
 Neutron Production ( $E < 50$  MeV) in an Infinite Uranium Target  
 for 20-, 50-, 100-, and 500-GeV Source Protons Using the HETC88 Code.

<u>Energy Type</u>	<u>Proton Energy (GeV)</u>			
	20.0	50.0	100.	500.
Primary ionization	0.296	0.248	0.284(0.310) <sup>d</sup>	0.247
Secondary protons	3.58	6.97	11.8(22.3)	45.4
Secondary charged pions <sup>a</sup>	2.05	5.27	9.84(7.11)	41.9
Secondary muons	0.008	0.021	0.041(0.097)	0.175
Excitation gammas <sup>b</sup>	0.197	0.411	0.697(1.26)	2.76
Neutral pions and high energy gammas	5.68	20.1	48.6(20.5)	293.
Heavy ion recoil	0.325	0.715	1.23(3.32)	5.08
Binding and neutrino energy and electron energy from muon decay	5.33	10.9	18.4(27.4)	74.4
Energy of neutrons produced with energy less than 50 MeV <sup>c</sup>	2.53	5.35	9.09(17.3)	36.7
Neutrons produced per GeV ( $E < 50$ MeV)	26.3	22.3	19.0(35.0)	15.3
Number of fast fissions <sup>e</sup>	39.9	82.0	138.(250.)	545.

<sup>a</sup> In this version of HETC, all kaons, anti-protons, etc., are converted to charged pions before transport.

<sup>b</sup> Energy remaining in nucleus after collisions involving all charged particles and neutrons with energies  $> 50$  MeV.

<sup>c</sup> This is the total energy contained in neutrons with energies less than 50 MeV. If these particles were transported until capture, the binding energy would reduce by  $\sim$  the number of neutrons times 7 MeV.

<sup>d</sup> Values in parentheses are those obtained using the old version of HETC. For energies less than 5 GeV, the old version of HETC is equivalent to the new version.

<sup>e</sup> Fissions produced by all charged particles and neutrons with energy  $> 50$  MeV. To calculate the amount of prompt fission gamma energy multiply by 7.538 MeV/fission. The energy associated with fission is not included for calculating binding energy.

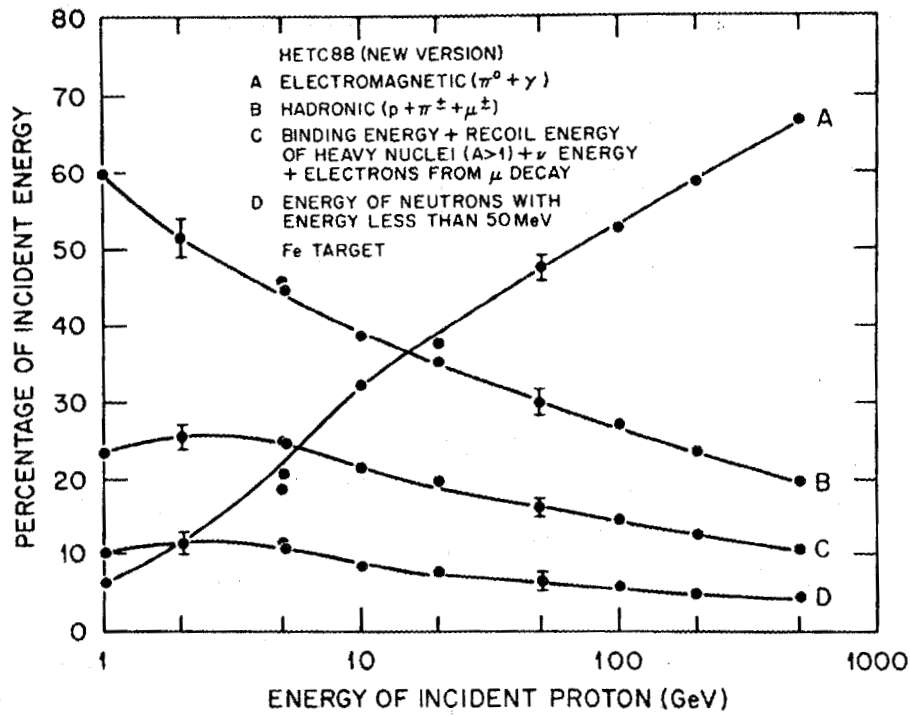


Fig. 2. Energy deposition and particle production percentage for an infinite iron target as a function of source proton energy (HETC88).

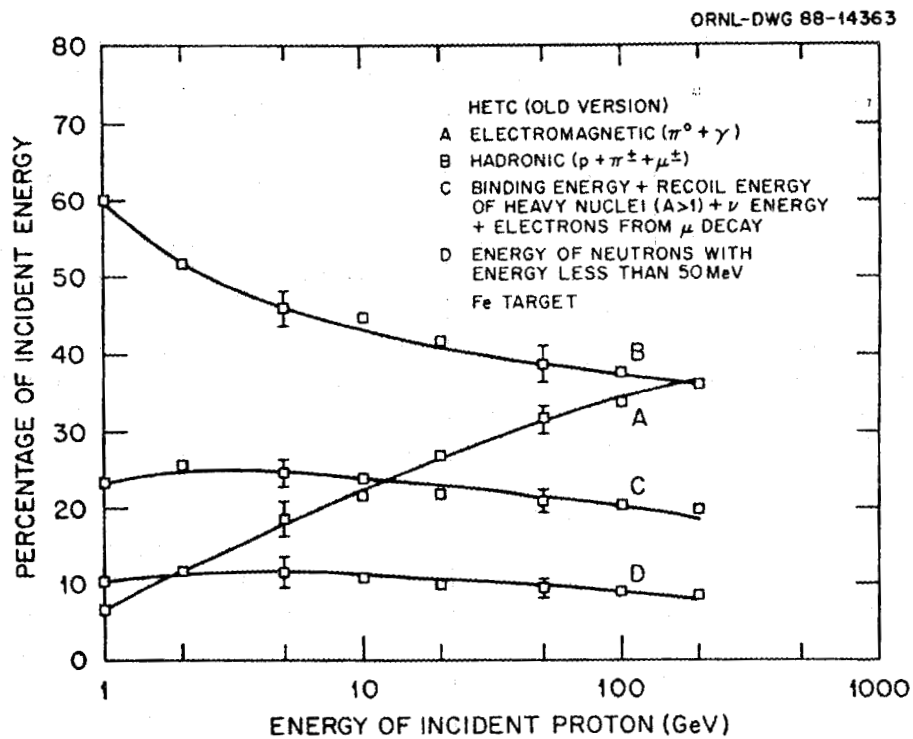


Fig. 3. Energy deposition and particle production percentage for an infinite iron target as a function of source proton energy (old HETC).

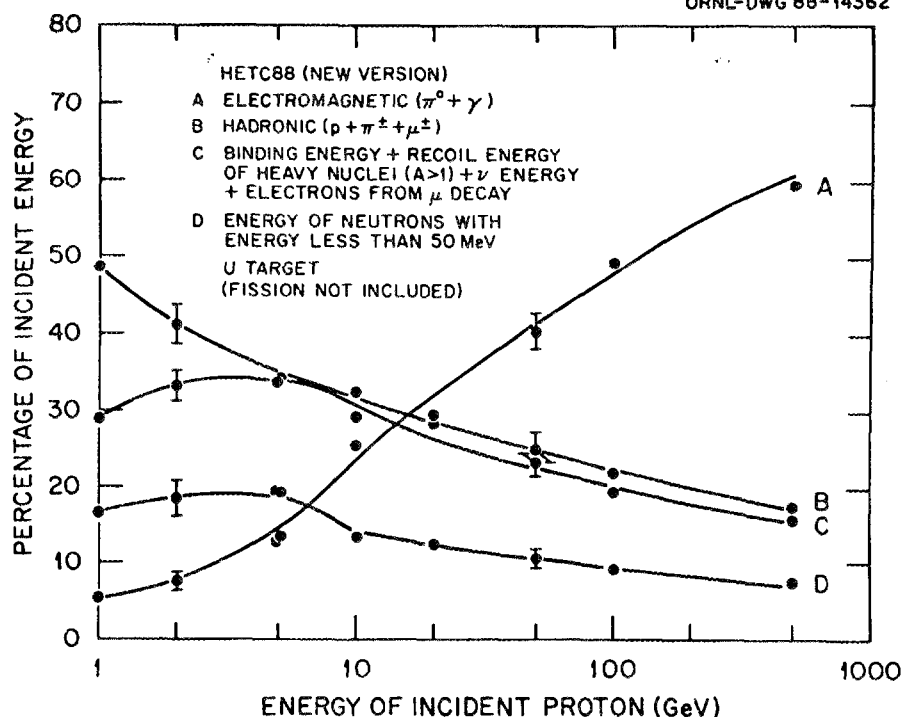


Fig. 4. Energy deposition and particle production percentage for an infinite uranium target as a function of source proton energy (HETC88).

The binding and neutrino energies are calculated by subtracting from the source proton energy all of the above modes of energy deposition and production.

For the uranium data, fission has been ignored in the calculation of the binding and neutrino energy losses. However, listed in the tables are the calculated number of fissions which are expected to occur due to charged particles at all energies and to neutrons with energies greater than 50 MeV. By multiplying these values by 7.538 MeV/fission, the prompt fission gamma energy can be obtained. It should be remembered, however, that the majority of the fissions,  $\sim 75\%$  of the total, occur with neutrons with energies between 1 and 50 MeV.

If the low energy ( $< 50$  MeV) neutrons were transported, a small amount of energy would be lost in binding due to nonelastic collisions. However, a reduction in binding energy would eventually show up due to neutron capture,  $\sim 7-8$  MeV/capture. But, the time frame for capture, microseconds to milliseconds, is beyond that for calorimeter application.

Presented in parentheses in some of the tables and in Fig. 3 are data obtained using the older version of the HETC code; that is, the version which relies totally on the scaling model for all collisions above 3 GeV. It has been known for some time that the scaling model overestimated the amount of energy in the hadronic channel and underestimated the amount in the electromagnetic channel. By comparing these channels in Figs. 2 and 3, it is apparent that the new model corrects this deficiency and from previous experience dealing with calorimeter calculations at high energies, appears to produce proper amounts of each. Detailed calculations at high energies on well studied calorimeters will help quantify the above statement.

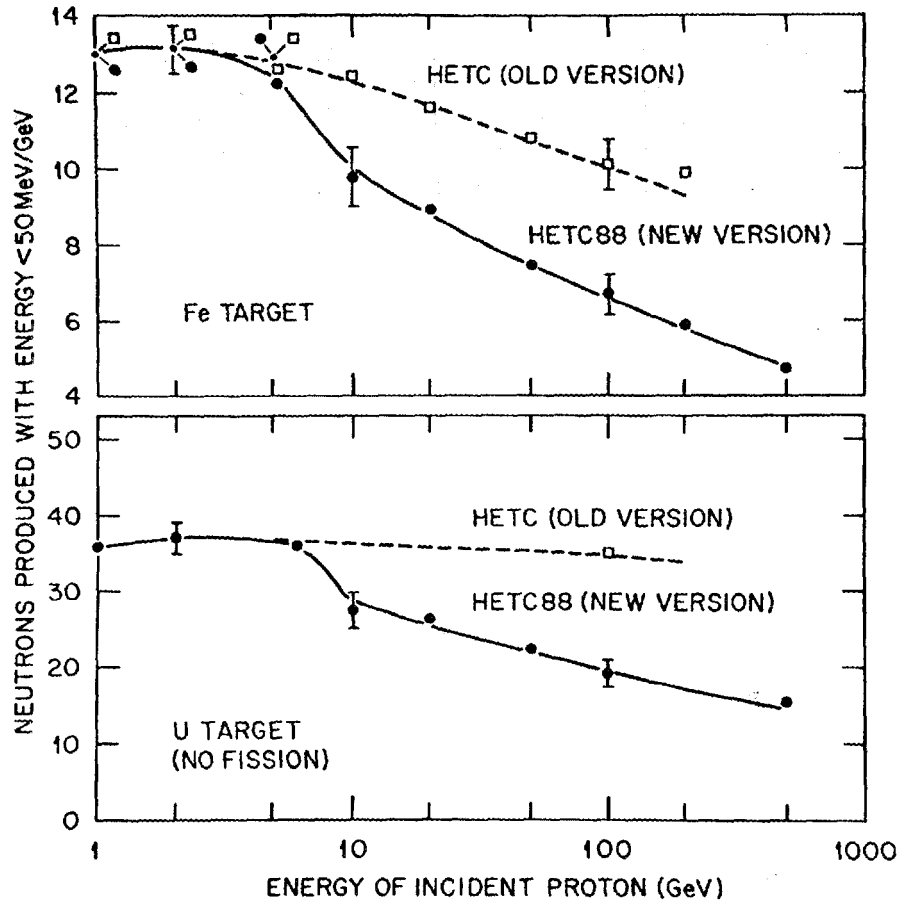


Fig. 5. Neutron production ( $E_N < 50$  MeV) in infinite iron and uranium targets as a function of source proton energy.

In the energy range from  $\sim 3$  GeV to  $\sim 20$  GeV, where the collision physics is slowly changing from "hard sphere individual nucleon scattering and immediate secondary particle production" to "jet formation and decay", the calculational bonding of the two model concepts is not totally complete. This is apparent by studying the data in this energy range. At present, an abrupt change is allowed to take place in the collision kinematics at 5 GeV rather than allowing for competing collision types, i.e., hard sphere scattering or jet formation. Methods are under study to unite the two different concepts of particle nucleus collision into a self-consistent model of nuclear cascades.

Presented in Fig. 5 is the number of neutrons produced per GeV of source particle energy for infinite iron and uranium targets. The production levels are important since they will determine the amount of radiation damage for SSC detectors. If the data were converted to neutrons/proton, and were plotted on log-log paper, the resulting graph would be fairly linear.

## 5. CONCLUSIONS

Large gains in the understanding of the physics of calorimetry have been accomplished in the past from the use of radiation transport code systems. A new revised version of CALOR, CALOR89, with several improved modules HETC88 and MICAP is about to be released which should strengthen our understanding and should allow for better calorimeter designs for the SSC.

## REFERENCES

1. T. A. Gabriel et al., "Compensation Effects in Hadron Calorimeters," *IEEE Trans. Nucl. Sci.* NS-32, 1 (1985).
2. J. E. Brau and T. A. Gabriel, SLD - New Detector Note No. 119, May 22, 1984.
3. J. E. Brau, "A Monte Carlo Investigation of Compensation in Uranium Calorimeters," *Proceedings of the September 1984 Seattle Meeting of the SLD Collaboration*.
4. T. A. Gabriel, "Codes, Models, and Cross Sections for Use in Analyzing Compensated Calorimeters," *Proceedings of Workshop on Compensated Calorimetry*, Pasadena (1985) CALT-68-1305.
5. J. Brau and T. A. Gabriel, "Monte Carlo Studies of Uranium Calorimetry," *Nucl. Instrum. & Methods* Vol. A238, p. 489, 1985.
6. J. Brau, "A Monte Carlo Investigation of Compensation in Uranium Calorimeters," *Proceedings of Workshop on Compensated Calorimetry*, Pasadena (1985) CALT-68-1305.
7. P. M. Mockett, *Proceedings of the 11th SLAC Summer Institute on Particle Physics*, July 1983, Ed. Patricia M. McDonough, SLAC-267, 1984.
8. H. Gordon and P. Grannis, "Calorimetry for the SSC," *Proceedings of the 1984 Summer Study on the Design and Utilization of the SSC*, Snowmass, Colorado, 1984, p. 591.
9. See *Proceedings of Workshop on Compensated Calorimetry*, Pasadena, California, 1985, CALT-68-1305.
10. H. Brüeckmann, "Hadron Calorimetry - A Puzzle of Physics," *Proceedings of Workshop on Compensated Calorimetry*, Pasadena, 1985, CALT-68-1305.
11. R. Wigmans, "On the Energy Resolution of Uranium and Other hadron Calorimeters," *Nucl. Instrum. & Methods* Vol. 259, p. 389, 1987.
12. J. E. Brau and T. A. Gabriel, "Theoretical Studies of High Luminosity, High Energy Colliders," presented at the *International Conference on Advanced Technology and Particle Physics*, Como, Italy, June 15, 1988, and to be published in *Nucl. Instrum. & Methods*.
13. R. G. Alsmiller, Jr. et al., "Modifications of the High-Energy Transport Code (HETC) and Comparisons with Experimental Results," *Proceedings of Conference on Theory and Practices in Radiation Protection and Shielding*, Knoxville, Tennessee, April 22-24, 1987.
14. J. B. Birks, *Proc. Phys. Soc.* Vol. A64, p. 874, 1951.
15. C. W. Fabjan et al., *Nucl. Instrum. & Methods* Vol. 141, p. 61, 1977.
16. T. A. Gabriel, "The High Energy Transport Code HETC," Oak Ridge National Laboratory, ORNL/TM-9727, 1985.

17. T. A. Gabriel et al., "CALOR87: HETC87, MICAP, EGS4, and SPECT, A Code System for Analyzing Detectors for Use in High Energy Physics Experiments," *Proceedings of the Workshop on Detector Simulation for the SSC*, Argonne National Laboratory, August 24-28, 1987.
18. The latest HETC code will be referred to as HETC88.
19. H. W. Bertini, *Phys. Rev.* Vol. 188, p. 1711, 1969.
20. P. A. Aarnio et al., CERN TIS Divisional Report, TIS-RP/106-ReV, 1984.
21. A. Capella and J. Tran Thanh Van, *Phys. Letts.* Vol. 93B, p. 2, June, 1980.
22. F. S. Alsmiller et al., "Low-Energy Particle Production and Residual Nuclei Production from High-Energy Hadron-Nucleus Collisions," *Proceedings of Conference on Theory and Practices in Radiation Protection and Shielding*, Knoxville, Tennessee, April 22-24, 1987.
23. R. J. Glauber, *Lectures in Theoretical Physics*, Ed. W. E. Brittin and L. G. Dunham, Vol. 1, (Interscience, NY), 1959.
24. V. N. Gribov, *Zh. Eksp. Teor. Fiz.* Vol. 57, p. 1306, 1969.
25. J. Ranft and S. Ritter, *Z. Phys. C - Particles and Fields* Vol. 20, p. 347, 1983.
26. G. Nilsson and E. Stenlund, Lund University Preprint, LU-TP8009, 1980.
27. A. Capella and A. Drzywicki, *Phys. Rev. D* Vol. 18, p. 3357, 1978.
28. J. Ranft and S. Ritter, *Z. Phys. C - Particles and Fields* Vol. 27, p. 569, 1985.
29. J. Ranft, CERN TIS Divisional Report TIS-RP/172/PP, 1986.
30. P. A. Aarnio et al., CERN TIS Divisional Report TIS-RP/168, 1986.
31. P. Aurenche et al., *Z. Phys. C - Particles and Fields* Vol. 23, p. 67, 1984.
32. S. Ritter and J. Ranft, *Acta Physica Polonica* Vol. B11, 1980.
33. K. Hanbgen and S. Ritter, Karl-Marx Universitat, Leipzig, DDR, KMU-HEP 8301, 1983.
34. R. L. Ford and W. R. Nelson, SLAC-0210, 1978.
35. M. B. Emmett, Oak Ridge National Laboratory, ORNL-4972, 1975.
36. N. M. Greene et al., Oak Ridge National Laboratory, ORNL/TM-3706, 1973.
37. J. O. Johnson and T. A. Gabriel, Oak Ridge National Laboratory, ORNL/TM-10196, 1987.
38. A. Babaev et al., *Nucl. Instrum. & Methods* Vol. 160, p. 427, 1979.

## INTERNAL DISTRIBUTION

- |                         |                              |
|-------------------------|------------------------------|
| 1. F. S. Alsmiller      | 15-19. C. Zeigler            |
| 2. R. G. Alsmiller, Jr. | 20. EPMD Reports Office      |
| 3. B. R. Appleton       | 21-22. Laboratory Records    |
| 4. D. E. Bartine        | Department                   |
| 5. B. L. Bishop         | 23. Laboratory Records,      |
| 6-10. T. A. Gabriel     | ORNL-RC                      |
| 11. J. K. Ingersoll     | 24. Document Reference       |
| 12. R. A. Lillie        | Section                      |
| 13. F. C. Maienschein   | 25. Central Research Library |
| 14. RSIC                | 26. ORNL Patent Section      |

## EXTERNAL DISTRIBUTION

27. Office of the Assistant Manager for Energy Research and Development, Department of Energy, Oak Ridge Operations, P.O. Box 2001, Oak Ridge, TN 37831
- 28-37. Office of Scientific and Technical Information, PO Box 62, Oak Ridge, TN 37830
38. Argonne National Laboratory, Library Services Dept., 302-CE125, 9700 S. Cass Avenue, Argonne, IL 60439
39. T. W. Armstrong, Science Applications, Inc., PO Box 2807, La Jolla, CA 92038
40. Miguel Awschalom, National Accelerator Laboratory, PO Box 500, Batavia, IL 60510
41. V. S. Barashenkov, Laboratory of Theoretical Physics, Joint Institute for Nuclear Research, Head Post Office, PO Box 79, Moscow, USSR
42. Gerald W. Bennett, Brookhaven National Laboratory, Upton, NY 19973
43. D. Berley, National Science Foundation, Washington, DC 20550
44. Elliott Bloom, Stanford Linear Accelerator Center, PO Box 4349, Stanford, CA 94305
45. J. Brau, University of Oregon, Eugene, OR 97403
46. Bruce Brown, Fermi National Accelerator Laboratory, PO Box 500, Batavia, IL 60510
47. David O. Caldwell, Dept. of Physics, University of California at Santa Barbara, Santa Barbara, CA 93106
48. Stanley B. Curtis, Lawrence Radiation Laboratory, Bldg. 29, Room 213, Berkeley, CA 94720
49. Herbert DeStaebler, Stanford Linear Accelerator Center, Stanford University, Stanford, CA 94305
50. A. Di Ciaccio, CERN, Geneva 23, Switzerland
51. Tom Dombeck, Div. of High Energy & Nucl. Phys., U. S. Dept. of Energy, 19901 Germantown Rd, Germantown, MD 20874
52. J. J. Dorning, Dept. of Nucl. Eng. and Engineering Physics, University of Virginia, Charlottesville, VA 22901
53. R. D. Edge, Physics Dept., University of South Carolina, Columbia, SC, 29208
54. R. Eisenstein, Dept. of Physics, University of Illinois, Urbana, IL 61801

55. R. W. Ellsworth, George Mason University, Fairfax, VA 22030
56. Chris Fabjan, CERN, Geneva 23, Switzerland
57. G. Feldman, Stanford Linear Accelerator Center, Stanford University, Stanford, CA 94305
58. W. T. Ford, Experiment 1A-Lab C, Fermi National Accelerator Laboratory, PO Box 500, Batavia, IL 60510
59. E. Fowler, Dept. of Physics, Purdue University, West Lafayette, IN 47907
60. H. T. Freudenreich, University of Maryland, College Park, MD 20742
61. E. Freytag, Deutsches Elektronen-Synchrotron, DESY, 2 Hamburg Dr., Flottbek, Notkesteig 1, W. Germany
62. A. F. Garfinkel, Purdue University, Dept. of Physics, W. Lafayette, IN 47907
63. M. G. D. Gilchriese, SSC Central Design Group, Lawrence Berkeley Laboratory, Berkeley, CA 94720
64. G. T. Gillies, Dept. of Physics, University of Virginia, Charlottesville, VA 22901
65. G. E. Gladding, University of Illinois, Dept. of Physics, Urbana, IL 61801
66. K. Goebel, Health Physics Group, CERN, 1211 Geneva 23, Switzerland
67. J. A. Goodman, University of Maryland, College Park, MD 20742
68. M. Goodman, Bell Communication Research, Morristown, NJ 07960
69. D. Groom, SSC Central Design Group, Lawrence Berkeley Laboratory, Berkeley, CA 94720
70. Herman Grunder, Deputy Director, General Sciences, Lawrence Berkeley Laboratory, Bldg. 50A, Room 4119, 1 Cyclotron Rd., Berkeley, CA 94720
71. H. J. Hargis, University of Tennessee, Dept. of Physics, Knoxville, TN 37919
72. Frenc Hajnal, Health and Safety Laboratory, U.S. Department of Energy, 376 Hudson St., New York, NY 120014
73. R. M. Haralick, Dept. of Electrical Engineering, University of Washington, Seattle, WA 98195
74. M. Hofert, CERN, 1211 Geneva 23, Switzerland
75. Terrence Jensen, Dept. of Physics and Astronomy, The University of Rochester, Rochester, NY 14627
76. D. Lal, Tata Institute of Fundamental Research, National Centre of the Government of India, for Nuclear Science & Mathematics, Homi Bhabha Rd., Bombay 5, India
77. Lawrence Livermore Laboratory, Technical Information Department, PO Box 808, Livermore, CA 94550
78. V. Lebedev, Institute of High Energy Physics, Serpukhov, Moscow Region, USSR
79. Library for Nuclear Science, Massachusetts Institute of Technology at Middleton, Middleton, MA 01949
80. J. LoSecco, Dept of Physics, California Institute of Technology, Pasadena, CA 91125
81. J. Marks, Accelerator Fusion Research Division, Lawrence Berkeley Laboratory, Bldg. 50, Room 149, 1 Cyclotron Rd., Berkeley, CA 94720
82. A. I. Mincer, University of Maryland, College Park, Md 20742
83. V. S. Narashimham, Tata Institue of Fundamental Research, Bombay 400 005,, India
84. W. R. Nelson, Stanford Linear Acclerator Center, Stanford University, PO Box 4349, Stanford, CA 94305

85. T. R. Palfrey, Jr., Dept. of Physics, Purdue University, West Lafayette, IN 47907
86. Robert Palmer, Brookhaven National Laboratory, Upton, NY 11973
87. C. W. Peck, Dept. of Physics, California Institute of Technology, Pasadena, CA 91109
88. J. Ranft, Karl-Marx University, Physics Section, Linnestrasse 5, 701, Leipzig, E. Germany
89. Lincoln Read, Division of High Energy & Nuclear Physics, Department of Energy, Washington, DC 20545
90. Jim Reidy, University of Mississippi, University, MS 38677
91. Enloe T. Ritter, Div. of High Energy & Nucl. Phys., U.S. Department of Energy, 19901 Germantown Rd, Germantown, Md 20874
92. C. Rubbia, Lyman Laboratory, Harvard University, Cambridge, MA 02138
93. W. Schmidt, Institute of Experimental Nuclear Physics, University of Karlsruhe, 75 Karlsruhe, W. Germany
94. The Secretary, Radiation Group, Lab II, CERN, 1211 Geneva 23, Switzerland
95. Walter Selove, University of Pennsylvania, Dept. of Physics, Philadelphia, PA 19104
96. B.S.P. Shen, Dept. of Astronomy, University of Pennsylvania, Philadelphia, PA 19104
97. M. Shupe, Dept. of Physics, University of Minnesota, Minneapolis, MN 55455
98. Alan Stevens, Physics Dept., Brookhaven National Laboratory, Upton, NY 11973
99. G. R. Stevenson, Radiation Protection Group, Lab II, CERN, 1211 Geneva 23, Switzerland
100. L. Sulak, Dept. of Physics, University of Michigan, Ann Arbor, MI 48109
101. R. F. Taschek, Los Alamos National Laboratory, PO Box 1663, Los Alamos, NM 87544
102. R. Tesch, DESY, Hamburg, Notkesteig 1, W. Germany
103. R. H. Thomas, Lawrence Radiation Laboratory, Health Physics Dept., Bldg. 72, Berkeley, CA 94720
104. V. D. Toneev, Laboratory of Theoretical Physics, Joint Institute for Nuclear Research, Head Post Office, PO Box 79, Moscow, USSR
105. S. C. Tonwar, University of Maryland, College Park, Md 20742
106. W. Turchinets, Massachusetts Institute of Technology, R26-411, Cambridge, MA 02139
107. Jim Walker, University of Florida, Gainesville, FL 32611
108. W. J. Willis, CERN, Geneva 23, Switzerland
109. D. Winn, Lyman Laboratory, Harvard University, Cambridge, MA 02138
110. J. Wilczynski, Nuclear Research Center, Karlsruhe, W. Germany
111. S. Yellin, Stanford University, Stanford Linear Accelerator Center, PO Box 4349, Stanford, CA 94305
112. G. B. Yodh, University of Maryland, College Park, MD 20742
113. S. Youssef, SCRI, Florida State University, Tallahassee, FL 32306
114. B. Zeitnitz, Nuclear Research Center, Karlsruhe, W. Germany